

We are IntechOpen, the world's leading publisher of Open Access books Built by scientists, for scientists

6,900

Open access books available

186,000

International authors and editors

200M

Downloads

Our authors are among the

154

Countries delivered to

TOP 1%

most cited scientists

12.2%

Contributors from top 500 universities



WEB OF SCIENCE™

Selection of our books indexed in the Book Citation Index
in Web of Science™ Core Collection (BKCI)

Interested in publishing with us?
Contact book.department@intechopen.com

Numbers displayed above are based on latest data collected.
For more information visit www.intechopen.com



Impurity Effects in Iron Pnictide Superconductors

Yuriy G. Pogorelov, Mario C. Santos and
Vadim M. Loktev

Additional information is available at the end of the chapter

<http://dx.doi.org/10.5772/59629>

1. Introduction

The recent discovery of superconductivity (SC) with rather high critical temperature in the family of doped iron pnictide compounds [1, 2], has motivated a great interest to these materials (see the reviews [3, 4]). Unlike the extensively studied cuprate family [5], that present insulating properties in their initial undoped state, the undoped LaOFeAs compound is a semimetal. As was established by the previous physical and chemical studies (see, e.g., [6, 7]), this material has a layered structure, where the SC state is supported by the FeAs layer with a 2D square lattice of Fe atoms and with As atoms located out of plane, above or below the centers of square cells (Fig. 1). Its electronic structure, relevant for constructing microscopic SC models, have been explored with high-resolution angle-resolved photoemission spectroscopy (ARPES) techniques [8, 9]. Their results indicate the multiple connected structure of Fermi surface, consisting of electron and hole pockets and absence of nodes in both electron and whole spectrum gaps [8], suggesting these systems to display the so-called extended s -wave (also called s_{\pm} -wave) SC order, changing the order parameter sign between electron and whole segments [10].

To study the band structure, the first principles numeric calculations are commonly used, outlining the importance of Fe atomic d -orbitals. The calculations show that SC in these materials is associated with Fe atoms in the layer plane, represented in Fig. 1 by their orbitals and the related hopping amplitudes. The dominance of Fe atomic $3d$ orbitals in the density of states of LaOFeAs compound near its Fermi surface was demonstrated by the local density approximation (LDA) calculations [10-15]. It was then concluded that the multi-orbital effects are important for electronic excitation spectrum in the SC state, causing formation of two spectrum gaps: by electron and hole pockets at the Fermi surface. To explain the observed SC properties, an unconventional pairing mechanism, beyond the common electron-phonon

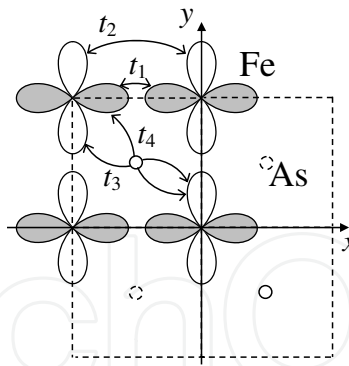


Figure 1. Schematics of a FeAs layer in the LaOFeAs compound with d_{xz} (dark) and d_{yz} (white) Fe orbitals and the Fe-Fe hopping parameters in the minimal coupling model. Note that the hoppings between next near neighbors ($t_{3,4}$) are mediated by the As orbitals (out of Fe plane)

scheme, was suggested for these materials [16-19]. In general, the total of 5 atomic orbitals for each iron in the LaOFeAs compound can be involved, however the ways to reduce this basis are sought, in order to simplify analytical and computational work. Some authors [20, 21] have suggested that it is sufficient to consider only the d_{xz} and d_{yz} orbitals. Building such minimal coupling model based on two orbitals, one is able to adjust the model parameters (energy hopping and chemical potential) to obtain the Fermi surface with the same topology that in the first principles calculations of band structure. Even though it fails to reproduce some finer features of the electronic spectrum [22, 23], this minimal coupling scheme is favored by its technical simplicity to be chosen as a basis for study of impurity effects in LaOFeAs which could be hardly tractable in more involved frameworks.

Having established the SC state parameters, important effects of disorder, in particular by impurities, on the system electronic properties, have been studied for doped iron pnictides. Alike the situation in doped perovskite cuprates, impurity centers can result here either from dopants, necessary to form the very SC state, or from foreign atoms and other local defects. Within the minimal coupling model, an interesting possibility for localized impurity levels within SC gaps in doped LaOFeAs was indicated, even for the simplest, so-called isotopic (or non-magnetic) type of impurity perturbation [24, 25]. This finding marks an essential difference from the traditional SC systems with s -wave gap on a single-connected Fermi surface, were such perturbations are known not to produce localized impurity states and thus to have no sizeable effect on SC order, accordingly to the Anderson theorem [26].

In presence of localized quasiparticle states by isolated impurity centers, the next important issue is the possibility for collective behavior of such states at finite (but low enough) impurity concentration. They are expected to give rise to some resonance effects like those well studied in semiconductors at low doping concentrations [27]. This possibility was studied long ago for electronic quasiparticles in doped semiconducting systems [28] and also for other types of quasiparticles in phononic, magnonic, excitonic, etc. spectra under impurities [29], establishing conditions for collective (including coherent) behavior of impurity excitations. Thus, indirect interactions between impurity centers of certain type (the so-called deep levels at high enough concentrations) in doped semiconductors can lead

to formation of collective band-like states [28, 30]. This corresponds to the Anderson transition in a general disordered system [31], and the emerging new band of quasiparticles in the spectrum can essentially change thermodynamics and transport in the doped material [32]. In this course, the fundamental distinction between two possible types of states is done on the basis of general Ioffe-Regel-Mott (IRM) criterion that a given excitation has a long enough lifetime compared to its oscillation period [32, 33].

Analogous effects in superconductors were theoretically predicted and experimentally discovered for magnetic impurities, both in BCS systems [34-36] and in the two-band MgB₂ system [37, 38]. In all those cases, the breakdown of the Anderson's theorem is only due to the breakdown of the spin-singlet symmetry of an *s*-wave Cooper pair by a spin-polarized impurity. This limitation does not apply to the high-*T_c* doped cuprates, however their *d*-wave symmetry of SC order only permits impurity resonances in the spectrum of quasiparticles [39, 40], not their true localization, and hinders notable collective effects on their observable properties.

Therefore the main physical interest in SC iron pnictides from the point of view of disorder in general is the possibility for pair-breaking even on non-magnetic impurity [41-43] and for related localized in-gap states [21, 44-46]. This theoretical prediction was confirmed by the observations of various effects from localized impurity states, for instance, in the superfluid density (observed through the London penetration length) [47, 48], transition critical temperature [49, 50] and electronic specific heat [51], all mainly due to an emerging spike of electronic density of states against its zero value in the initial band gap. An intriguing possibility for banding of impurity levels within the SC gap [38, 52], similar to that in the above mentioned normal systems, was recently discussed for doped iron pnictides [53]. Here a more detailed analysis of the band-like impurity states is also focused on their observable effects that cannot be produced by localized impurity states.

We apply the Green function (GF) techniques, similar to those for doped cuprate SC systems [54], using the minimal coupling model by two orbitals for host electronic structure and the simplest isotopic type for impurity perturbation. The energy spectrum near in-gap impurity levels at finite impurity concentrations, emergence of specific branches of collective excitations in this range, and expected observable effects of such spectrum restructuring are discussed. Then specific GFs for SC quasiparticles are used in the general Kubo-Greenwood formalism [55, 56] to obtain the temperature and frequency dependences of optical conductivity. These results are compared with available experimental data and some suggestions are done on possible practical applications.

2. Model Hamiltonian and Green functions

For the minimal coupling model of Fig. 1, the hopping Hamiltonian H_t is written in the local orbital basis as:

$$\begin{aligned}
H_t = & - \sum_{\mathbf{n}, \sigma} \left[t_1 \left(x_{\mathbf{n}, \sigma}^\dagger x_{\mathbf{n} + \delta_x, \sigma} + y_{\mathbf{n}, \sigma}^\dagger y_{\mathbf{n} + \delta_y, \sigma} + h.c. \right) + t_2 \left(x_{\mathbf{n}, \sigma}^\dagger x_{\mathbf{n} + \delta_y, \sigma} + y_{\mathbf{n}, \sigma}^\dagger y_{\mathbf{n} + \delta_x, \sigma} + h.c. \right) \right. \\
& + t_3 \left(x_{\mathbf{n}, \sigma}^\dagger x_{\mathbf{n} + \delta_x + \delta_y, \sigma} + x_{\mathbf{n}, \sigma}^\dagger x_{\mathbf{n} + \delta_x - \delta_y, \sigma} + y_{\mathbf{n}, \sigma}^\dagger y_{\mathbf{n} + \delta_x + \delta_y, \sigma} + y_{\mathbf{n}, \sigma}^\dagger y_{\mathbf{n} + \delta_x - \delta_y, \sigma} + h.c. \right) \\
& \left. + t_4 \left(x_{\mathbf{n}, \sigma}^\dagger y_{\mathbf{n} + \delta_x + \delta_y, \sigma} + y_{\mathbf{n}, \sigma}^\dagger x_{\mathbf{n} + \delta_x + \delta_y, \sigma} - x_{\mathbf{n}, \sigma}^\dagger y_{\mathbf{n} + \delta_x - \delta_y, \sigma} - y_{\mathbf{n}, \sigma}^\dagger x_{\mathbf{n} + \delta_x - \delta_y, \sigma} + h.c. \right) \right]. \quad (1)
\end{aligned}$$

where $x_{\mathbf{n}, \sigma}$ and $y_{\mathbf{n}, \sigma}$ are the Fermi operators for d_{xz} and d_{yz} Fe orbitals with spin σ on \mathbf{n} lattice site and the vectors $\delta_{x,y}$ point to its nearest neighbors in the square lattice. Passing to the operators of orbital plane waves $x_{\mathbf{k}, \sigma} = N^{-1/2} \sum_{\mathbf{n}} e^{i\mathbf{k} \cdot \mathbf{n}} x_{\mathbf{n}, \sigma}$ (N is the number of lattice cells) and analogous $y_{\mathbf{k}, \sigma}$ and defining an "orbital" 2-spinor $\psi_{\mathbf{k}, \sigma} = (x_{\mathbf{k}, \sigma}, y_{\mathbf{k}, \sigma})$, one expands the spinor Hamiltonian in quasimomentum:

$$H_t = \sum_{\mathbf{k}, \sigma} \psi_{\mathbf{k}, \sigma}^\dagger \hat{h}_t(\mathbf{k}) \psi_{\mathbf{k}, \sigma}. \quad (2)$$

Here the 2×2 matrix

$$\hat{h}_t(\mathbf{k}) = \varepsilon_{+,k} \hat{\sigma}_0 + \varepsilon_{-,k} \hat{\sigma}_3 + \varepsilon_{xy,k} \hat{\sigma}_1 \quad (3)$$

includes the Pauli matrices $\hat{\sigma}_i$ acting on the orbital indices and the energy functions

$$\varepsilon_{\pm,k} = \frac{\varepsilon_{x,k} \pm \varepsilon_{y,k}}{2}, \quad (4)$$

with

$$\begin{aligned}
\varepsilon_{x,k} &= -2t_1 \cos k_x a - 2t_2 \cos k_y a - 4t_3 \cos k_x a \cos k_y a, \\
\varepsilon_{y,k} &= -2t_1 \cos k_y a - 2t_2 \cos k_x a - 4t_3 \cos k_x a \cos k_y a, \\
\varepsilon_{xy,k} &= -4t_4 \sin k_x a \sin k_y a,
\end{aligned}$$

(a is the distance between nearest neighbor Fe). An optimum fit for the calculated band structure in the minimum coupling model is with the hopping parameters (in $|t_1|$ units): $t_1 = -1.0$, $t_2 = 1.3$, $t_3 = t_4 = -0.85$, and with the Fermi energy $\varepsilon_F = 1.45$ [15]. A unitary transformation brings $\hat{h}_t(\mathbf{k})$ from orbital to diagonal subband basis:

$$\hat{h}_b(\mathbf{k}) = \hat{U}^\dagger(\mathbf{k}) \hat{h}_t(\mathbf{k}) \hat{U}(\mathbf{k}) = \varepsilon_{e,k} \hat{\sigma}_+ + \varepsilon_{h,k} \hat{\sigma}_-, \quad \hat{U}_k = e^{-i\hat{\sigma}_2 \theta_k / 2}. \quad (5)$$

Here $\theta_k = \arctan(\varepsilon_{xy,k} / \varepsilon_{-,k})$, $\sigma_{\pm} = (\sigma_0 \pm \sigma_3) / 2$, and the energy eigenvalues:

$$\varepsilon_{h,e}(\mathbf{k}) = \varepsilon_{+,k} \pm \sqrt{\varepsilon_{xy,k}^2 + \varepsilon_{-,k}^2}, \quad (6)$$

correspond to the two subbands in the normal state spectrum that respectively define electron and hole pockets of the Fermi surface. There are two segments of each type, defined by the equations $\varepsilon_{e,h}(\mathbf{k}) = \mu$, as shown in Fig. 2. We note that both functions $\cos\theta_k$ and $\sin\theta_k$ change their sign around each of these segments, corresponding to their "azimuthal dependencies" around the characteristic points of the 2D Brillouin zone (Fig. 2), so that integrals of these functions with some azimuthal-independent factors over the relevant vicinity of Fermi surface practically vanish and are neglected beside the integrals of fully azimuthal-independent functions in the analysis below.

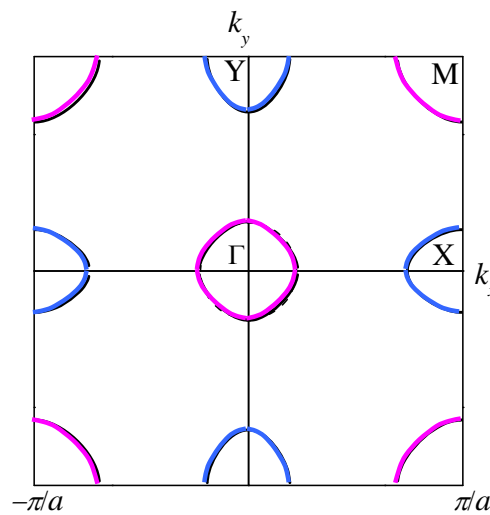


Figure 2. Electron (pink) and hole (blue) segments of the Fermi surface in the normal state of model system with electronic spectrum by Eq. 5. The dashed line around the Γ point marks a circular approximation (see after Eq. 11).

The adequate basis for constructing the SC state is generated by the operators of electron and hole subbands:

$$\begin{aligned} \alpha_{k,\sigma} &= x_{k,\sigma} \cos\theta_k / 2 - y_{k,\sigma} \sin\theta_k / 2, \\ \beta_{k,\sigma} &= y_{k,\sigma} \cos\theta_k / 2 + x_{k,\sigma} \sin\theta_k / 2, \end{aligned} \quad (7)$$

giving rise to the "multiband-Nambu" 4-spinors $\Psi_k^\downarrow = (\alpha_{k,\uparrow}^\downarrow, \alpha_{-k,\downarrow}^\downarrow, \beta_{k,\uparrow}^\downarrow, \beta_{-k,\downarrow}^\downarrow)$ and to a 4×4 extension of the Hamiltonian Eq. (2) in the form:

$$H_s = \sum_{k,\sigma} \Psi_k^\dagger \hat{h}_s(\mathbf{k}) \Psi_k, \quad (8)$$

where the 4×4 matrix

$$\hat{h}_s(\mathbf{k}) = \hat{h}_b(\mathbf{k}) \otimes \hat{\tau}_3 + \Delta_k \hat{\sigma}_0 \otimes \hat{\tau}_1,$$

includes the Pauli matrices $\hat{\tau}_i$ acting on the Nambu (particle-antiparticle) indices in Ψ -spinors and $\hat{h}_b(k)$ is defined by Eq. (5). The simplified form for the extended s -wave SC order is realized with the definition of the gap function by constant values, $\Delta_k = \Delta$ on the electron segments and $\Delta_k = -\Delta$ on the hole segments.

The electronic dynamics of this system is determined by the (Fourier transformed) GF 4×4 matrices [58, 29, 54]:

$$\hat{G}_{k,k'} = \langle\langle \Psi_k | \Psi_{k'}^\dagger \rangle\rangle = i \int_{-\infty}^0 dt e^{i\varepsilon t/\hbar} \langle \Psi_k(t), \Psi_{k'}(0)^\dagger \rangle, \quad (9)$$

whose energy argument ε is understood as $\varepsilon - i0$ and $\langle A(t), B(0) \rangle$ is the quantum statistical average with Hamiltonian H of the anticommutator of Heisenberg operators. From the equation of motion:

$$\varepsilon \hat{G}_{k,k'} = \hbar \delta_{k,k'} \hat{\sigma}_0 \otimes \hat{\tau}_0 + \langle\langle [\Psi_k, H] | \Psi_{k'}^\dagger \rangle\rangle, \quad (10)$$

the explicit GF for the unperturbed SC system with the Hamiltonian H_s , Eq. (8), is diagonal in quasimomentum, $\hat{G}_{k,k'} = \delta_{k,k'} \hat{G}_k^0$, with the diagonal term:

$$\hat{G}_k^0 = \frac{\varepsilon \hat{\tau}_0 + \varepsilon_{e,k} \hat{\tau}_3 + \Delta \hat{\tau}_1}{2D_{e,k}} \otimes \hat{\sigma}_+ + \frac{\varepsilon \hat{\tau}_0 + \varepsilon_{h,k} \hat{\tau}_3 - \Delta \hat{\tau}_1}{2D_{h,k}} \otimes \hat{\sigma}_-, \quad (11)$$

where the denominators $D_{i,k} = \varepsilon^2 - \varepsilon_i^2(\mathbf{k}) - \Delta^2$ for $i = e, h$. Below we refer energy to the Fermi level ε_F , approximate the segments of Fermi surface by circles of radius k_i around the characteristic points K_i in the Brillouin zone, and linearize the dispersion laws near the Fermi level as $\varepsilon_j(\mathbf{k}) = \varepsilon_F + \xi_{j,k}$ with $\xi_{j,k} \approx \hbar v_j (|\mathbf{k} - \mathbf{K}_j| - k_j)$. Though the Fermi wavenumbers k_j and related Fermi velocities v_j for $j = e, h$ can somewhat differ at given hopping parameters and chemical potential, we shall neglect this difference and consider single values $k_j = k_F$ and $v_j = v_F$.

3. Impurity perturbation and self-energy

We pass to the impurity problem where local perturbation terms due to non-magnetic impurities [24] on random sites p in Fe square lattice with an on-site energy shift V :

$$H_{imp} = V \sum_{p,\sigma} (x_{p,\sigma}^\dagger x_{p,\sigma} + y_{p,\sigma}^\dagger y_{p,\sigma}), \quad (12)$$

are added to the Hamiltonian H_s . Without loss of generality, the parameter V can be taken positive, and this perturbation is suitably expressed in the multiband-Nambu basis:

$$H_{imp} = \frac{1}{N} \sum_{p,k,k'} e^{i(k'-k) \cdot p} \Psi_k^\dagger \hat{V}_{k,k'} \Psi_{k'} \quad (13)$$

through the 4x4 scattering matrix $\hat{V}_{k,k'} = V \hat{U}_k^\dagger \hat{U}_{k'} \otimes \hat{\tau}_3$. From Eq. (5) for \hat{U}_k , this matrix involves either "intra-band" and "inter-band" elements [41]. The latter scattering could lead to a transition from s_\pm to a competing s_{++} SC order (with the same sign of order parameter on both Fermi pockets) under impurity effect [43]. However, as shown below, such a possibility is effectively eliminated for the chosen local perturbation type, due to the specific quasimomentum k -dependence of the scattering elements, unlike their constancy postulated in Ref. [43].

Following Refs. [29, 53], the solution for Eq. (10) with the perturbed Hamiltonian $H_s + H_i$ can be obtained in different forms, suitable for different types of states, band-like (extended) or localized. All these forms result from the basic equation of motion:

$$\hat{G}_{k,k'} = \delta_{k,k'} \hat{G}_k^0 + \frac{1}{N} \sum_{p,k''} e^{i(k''-k) \cdot p} \hat{G}_k^0 \hat{V}_{k,k''} \hat{G}_{k'',k'} \quad (14)$$

by specific routines of its iterating for the "scattered" GF's $\hat{G}_{k'',k'}$. Thus, the algorithm, where the next iteration step *never* applies to the scattered GF's already present after previous steps, e.g., to that with $k'' = k$ in Eq. (14), leads to the so-called fully renormalized form (RF), suitable for band-like states. Its result for the most relevant diagonal GF $\hat{G}_k \equiv \hat{G}_{k,k}$ reads:

$$\hat{G}_k = \left[\left(\hat{G}_k^0 \right)^{-1} - \hat{\Sigma}_k \right]^{-1}, \quad (15)$$

where the self-energy matrix $\hat{\Sigma}_k$ is expressed by the related group expansion (GE):

$$\hat{\Sigma}_k = c \hat{T}_k \left(1 + c \hat{B}_k + \dots \right). \quad (16)$$

Here $c = \sum_p N^{-1}$ is the impurity concentration (per Fe site) and the T-matrix results from all the multiple scatterings by a single impurity:

$$\hat{T}_k = \hat{V}_{k,k} + \frac{1}{N} \sum_{k' \neq k} \hat{V}_{k,k'} \hat{G}_{k'}^0 \hat{V}_{k',k} + \frac{1}{N^2} \sum_{k' \neq k} \sum_{k'' \neq k, k'} \hat{V}_{k,k'} \hat{G}_{k'}^0 \hat{V}_{k',k''} \hat{G}_{k''}^0 \hat{V}_{k'',k} + \dots \quad (17)$$

The next term to the unity in the brackets in Eq. (16):

$$\hat{B}_k = \sum_n \left(\hat{A}_n e^{-ik \cdot n} + \hat{A}_n \hat{A}_{-n} \right) \left(1 + \hat{A}_n \hat{A}_{-n} \right)^{-1}, \quad (18)$$

describes the effects of indirect interactions in pairs of impurities, separated by vector \mathbf{n} , in terms of interaction matrices $\hat{A}_{\mathbf{n}} = \hat{T} \sum_{\mathbf{k} \neq \mathbf{k}'} e^{i\mathbf{k}' \cdot \mathbf{n}} \hat{G}_{\mathbf{k}'}$. Besides this restriction on summation, multiple sums in the products like $A_{\mathbf{n}} A_{-\mathbf{n}}$ never contain coincident quasimomenta. Eq. (18) presents the first non-trivial GE term and its other terms omitted in Eq. (16) relate to the groups of three and more impurities [29].

An alternative iteration routine applies Eq. (14) to *all* the scattered GF's, leading to the so-called non-renormalized form (NRF), suitable for localized states:

$$\hat{G}_{\mathbf{k}} = \hat{G}_{\mathbf{k}}^0 + \hat{G}_{\mathbf{k}}^0 \hat{\Sigma}_{\mathbf{k}}^0 \hat{G}_{\mathbf{k}}^0, \quad (19)$$

The NRF self-energy admits a GE: $\hat{\Sigma}_{\mathbf{k}}^0 = c \hat{T}_{\mathbf{k}}^0 (1 + c \hat{B}_{\mathbf{k}}^0 + \dots)$, that differs from the RF one by no restrictions in \mathbf{k} -sums for T-matrix, interaction matrices $\hat{A}_{\mathbf{n}}^0 = \hat{T}_{\mathbf{k}}^0 \sum_{\mathbf{k}'} e^{i\mathbf{k}' \cdot \mathbf{n}} \hat{G}_{\mathbf{k}'}^0$, and their products.

At the first step, we restrict GE to the common T-matrix level to find the possibilities for localized quasiparticle states and related in-gap energy levels by single impurities [21]. Next, at finite impurity concentrations, formation of (narrow) energy bands of specific collective states near these levels is studied. Finally, the criteria for such collective states to really exist in the disordered SC system follow from the analysis of non-trivial GE terms. We notice that RF for GF's $\hat{G}_{\mathbf{k}}$, in the above interaction matrices is just necessary for adequate treatment of interaction effects within the in-gap bands. To simplify the T-matrix, Eq. (17), note that $\hat{V}_{\mathbf{k},\mathbf{k}} = V \hat{\sigma}_0 \otimes \hat{\tau}_3$ and use the integrated GF matrix:

$$\hat{G}_0 = \frac{1}{N} \sum_{\mathbf{k}} \hat{U}_{\mathbf{k}} \hat{G}_{\mathbf{k}}^0 \hat{U}_{\mathbf{k}}^\dagger = \varepsilon [g_e(\varepsilon) \hat{\sigma}_+ + g_h(\varepsilon) \hat{\sigma}_-] \otimes \hat{\tau}_0.$$

This diagonal form (restricted only to the "inband" matrix elements) follows from the aforementioned cancellation of integrals with $\cos\theta_{\mathbf{k}}$ and $\sin\theta_{\mathbf{k}}$ in the "interband" matrix elements of $\hat{U}_{\mathbf{k}} \hat{G}_{\mathbf{k}}^0 \hat{U}_{\mathbf{k}}^\dagger$. This permits to consider below the SC order unchanged under the impurity effects.

The functions $g_j(\varepsilon) = N^{-1} \sum_{\mathbf{k}} D_{j,\mathbf{k}}^{-1}$ for $j = e, h$ are approximated near ε_F , $|\varepsilon - \varepsilon_F| \delta \Delta$, as:

$$g_j(\varepsilon) \approx -\frac{\pi \rho_j}{\sqrt{\Delta^2 - \varepsilon^2}}. \quad (20)$$

Here $\rho_j = m_j a^2 / (2\pi \hbar^2)$ are the Fermi densities of states for respective subbands (in parabolic approximation for their dispersion laws), and by the assumed identity of the Fermi segments they can be also considered identical $\rho_j = \rho_F$, so that $g_j(\varepsilon) = g(\varepsilon) = -\pi \rho_F / \sqrt{\Delta^2 - \varepsilon^2}$. Omitted terms in Eq. (20) are of higher orders in the small parameter $\varepsilon / \varepsilon_F \ll 1$. Then the momentum independent T-matrix is explicitly written as:

$$\hat{T}(\varepsilon) = \frac{V}{1+v^2} \frac{\varepsilon^2 - \Delta^2 + v\varepsilon\sqrt{\Delta^2 - \varepsilon^2} \hat{t}_3}{\varepsilon^2 - \varepsilon_0^2}, \quad (21)$$

it presents two symmetric poles within the gap, at $\varepsilon = \pm \varepsilon_0 = \pm \Delta / \sqrt{1+v^2}$ [21], with the dimensionless impurity perturbation parameter $v = \pi\rho_F V$. Near these poles, Eq. (21) can be approximated as:

$$\hat{T}(\varepsilon) \approx \gamma^2 \frac{\varepsilon - \varepsilon_0 \hat{t}_3}{\varepsilon^2 - \varepsilon_0^2}, \quad (22)$$

where $\gamma^2 = V\Delta v^2 / (1+v^2)^{3/2}$ is the effective constant of coupling between localized and band quasiparticles. At finite c , this T-matrix can be used in Eqs. (16) and (15) and then in the formal dispersion equation: $\text{Redet} \hat{G}_k^{-1} = 0$ [57], to obtain the dispersion laws of perturbed SC system in terms of the normal quasiparticles dispersion $\xi_k = \varepsilon_k - \varepsilon_F \equiv \xi$. They follow from the general expression: $\text{Re}(\tilde{\varepsilon}^2 - \Delta^2 - \xi^2) = 0$, with $\tilde{\varepsilon} = \varepsilon \left(1 - cVv\sqrt{1 - \varepsilon^2/\Delta^2} / (\varepsilon^2/\varepsilon_0^2 - 1) \right)$ and $\xi = \xi + cV(\varepsilon^2/\Delta^2 - 1) / (\varepsilon^2/\varepsilon_0^2 - 1)$, and display a peculiar multiband structure shown in Fig. 3.

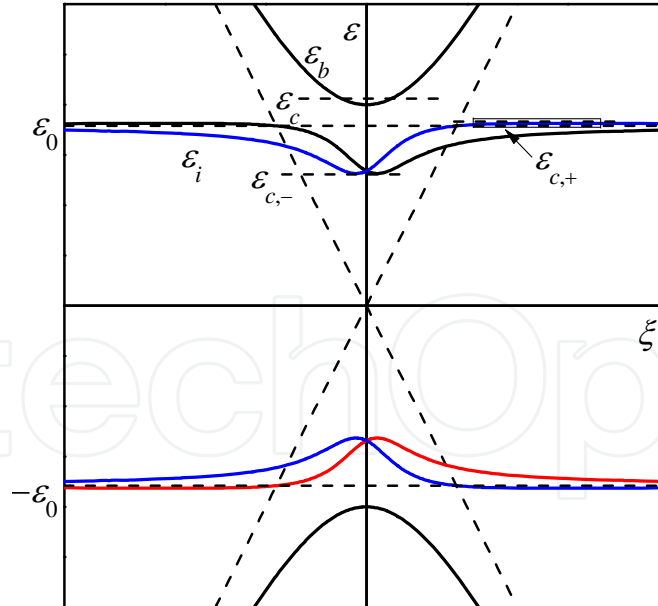


Figure 3. Dispersion laws for band-like quasiparticles in the T-matrix approximation, neglecting their finite lifetime, at a specific choice of impurity parameters $v = 1$, $c = 0.1\Delta^2/\gamma^2$. The argument ξ composes all specific $\xi_j = \hbar v_F (|\mathbf{k} - \mathbf{K}_j| - k_F)$ for \mathbf{k} near each j -th characteristic point in the Brillouin zone (see in the text), blue lines are for impurity bands near electron-like Fermi segments and red lines do for those near hole-like segments. The single-impurity localized levels are shown with dashed lines. The narrow rectangle around the top of ε_i -band (shown by the arrow) delimits the region in Fig. 5.

First of all, there are modified initial bands

$$\varepsilon_b(\xi) \approx \varepsilon(\xi) + i\Gamma(\xi), \quad (23)$$

whose main difference from the unperturbed SC bands with dispersion $\varepsilon(\xi) = \sqrt{\Delta^2 + \xi^2}$ is a finite linewidth $\Gamma(\xi) \sim cVv\xi\Delta/[(1+v^2)(\xi^2 + \xi_0^2)]$, $\xi_0^2 = \Delta^2 - \varepsilon_0^2$, defined by the T-matrix term of the self-energy, Eq. (16). It should be noted that these subbands for opposite signs of their argument ξ in fact refer to excitations around different Fermi segments (by electron and holes), but for clarity all four ε_b bands are set in Fig. 3 in the same ξ -reference. Then from the IRM criterion of band-like states:

$$\xi \frac{\partial}{\partial \xi} \varepsilon_b(\xi) \leftrightarrow \Gamma(\xi), \quad (24)$$

the position of mobility edge ε_c for these bands is estimated as: $\varepsilon_c - \Delta \sim (c/c_1)^2\Delta$, with $c_1 = \pi\rho_F\Delta \ll 1$. Besides the ε_b bands, there appear also four (narrow) in-gap ε_i bands, generated close to ε_0 at finite concentration of impurities, accordingly to:

$$\varepsilon_i(\xi) \approx \varepsilon_0 + c\gamma^2 \frac{\xi - \varepsilon_0}{\xi^2 + \xi_0^2}, \quad (25)$$

As follows from Eq. (25), the ε_i band has its extrema $\varepsilon_{max} = \varepsilon_0 + c\gamma^2/(\Delta + \varepsilon_0)$ at $\xi_+ = \Delta + \varepsilon_0$ and $\varepsilon_{min} = \varepsilon_0 - c\gamma^2/(\Delta - \varepsilon_0)$ at $\xi_- = \Delta - \varepsilon_0$. The energy and momentum shifts of these extremal points seen in Fig. 3 specify the impurity effect on a multiband initial spectrum, compared to a simpler situation for an impurity level near the edge of a single quasiparticle band [29].

All these spectrum bands would contribute to the overall density of states (DOS) by the related quasiparticles: $\rho(\varepsilon) = (4\pi N)^{-1} \text{Im Tr} \sum_k \hat{G}_k$. More common contributions there come from the ε_b bands and they can be expressed through the Bardeen-Cooper-Schrieffer (BCS) DOS in pure crystal [57]: $\rho_{\text{BCS}}(\varepsilon, \Delta) = \rho_F \varepsilon / \sqrt{\varepsilon^2 - \Delta^2}$, as follows:

$$\rho_b(\varepsilon) \approx \rho_{\text{BCS}}(\varepsilon, \Delta) - \frac{2c v^2 \varepsilon \sqrt{\varepsilon^2 - \Delta^2}}{\pi \varepsilon_F (1 + v^2) (\varepsilon^2 - \varepsilon_0^2)}, \quad (26)$$

at $\varepsilon^2 \rightarrow \varepsilon_c^2$. The second term in the r.h.s. of Eq. (26) describes a certain reduction of the BCS DOS at energies farther from the gap limits.

More peculiar contributions to DOS come from the ε_i bands, written as:

$$\rho_i(\varepsilon) \approx \frac{\rho_F}{v} \frac{\varepsilon^2 - \varepsilon_0^2 - c\gamma^2}{\sqrt{(\varepsilon_{max}^2 - \varepsilon^2)(\varepsilon^2 - \varepsilon_{min}^2)}}, \quad (27)$$

at $\varepsilon_{min}^2 \uparrow \varepsilon^2 \uparrow \varepsilon_{max}^2$, and presented in Fig. 4.

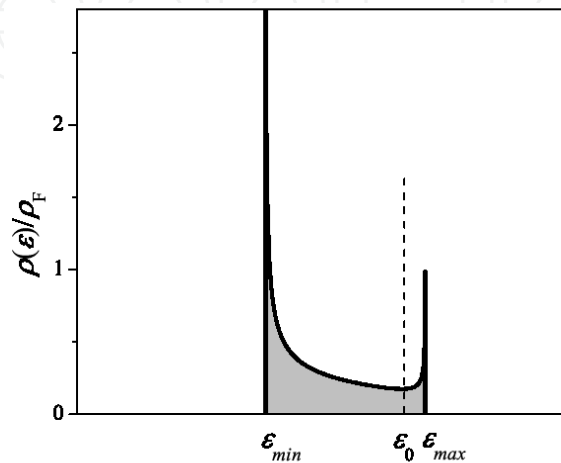


Figure 4. Density of states in the narrow in-gap band near the impurity level ε_0 (dashed line) for the case by Fig. 3.

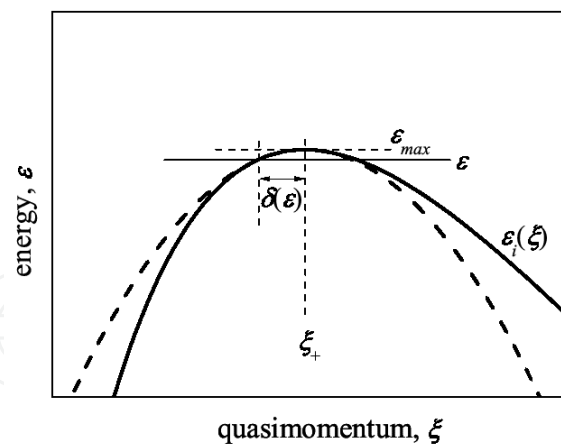


Figure 5. Parabolic approximation (dashed line) for the dispersion law near the top of impurity band (solid line), within the region indicated by a small rectangle in Fig. 3.

Formation of the ε_i bands can have important repercussions in the physical behavior of a disordered SC system and they will be considered below. But before this, we need to analyze the criteria for the considered quasiparticles to really exist, especially in closeness to the limits of corresponding bands and this requires a more involved analysis of non-trivial GE terms for self-energy.

4. Group expansion and Ioffe-Regel-Mott criteria

Let us now study the crossover from band-like to localized states near the limits of ε_i bands, say for definiteness, near its upper limit ε_{max} . Supposing the actual energy $\varepsilon < \varepsilon_{max}$ to be within the range of band-like states, we use the RF self-energy matrix, Eq. (16), up to the GE pair term, $c^2 \hat{T} \hat{B}_k$, that will add a certain finite imaginary part $\Gamma_i(\varepsilon)$ to the dispersion law $\varepsilon = \varepsilon_i(\xi)$, Eq. (25). Then the IRM criterion for a state at this energy be really band-like (also called extended) is written as:

$$\varepsilon_{max} - \varepsilon \gg \Gamma_i(\varepsilon). \quad (28)$$

To simplify calculation of the scalar function $\Gamma_i(\varepsilon)$, we fix the energy argument in the numerators of T-matrix and interaction matrices at $\varepsilon = \varepsilon_0$, obtaining their forms:

$$\hat{T}(\varepsilon) \approx \frac{\gamma^2 \varepsilon_0}{\varepsilon^2 - \varepsilon_0^2} \hat{m}_+, \quad \hat{A}_n(\varepsilon) \approx \hat{T}(\varepsilon) \frac{\varepsilon}{N} \sum_k \frac{e^{ik \cdot n}}{D_k(\varepsilon)}, \quad (29)$$

both proportional to the matrix $\hat{m}_+ = \hat{\sigma}_0 \otimes (\hat{\tau}_0 + \hat{\tau}_3)$ with important multiplicative property: $\hat{m}_+^2 = 2\hat{m}_+$. The k -summation (integration) in Eq. (29) is suitably done in polar coordinates over the circular segments of Fermi surface. Here the azimuthal integration only refers to the phase

of numerator, resulting in zeroth order Bessel function: $\int_0^{2\pi} e^{ix \cos \theta} d\theta = 2\pi J_0(x)$. Since $x = n(k_F + \xi/$

$\hbar v_F)$ is typically big, $x \gg 1$, the asymptotical formula applies: $J_0(x) \approx \sqrt{2/\pi x} \cos(x - \pi/4)$. Then, for radial integration in ξ around the extremum point ξ_+ , it is convenient to decompose this function into fast and slow oscillating factors: $J_0(x) \approx \sqrt{2/(\pi k_+ n)} \cos(k_+ n - \pi/4) \cos[(\xi - \xi_+)n/\hbar v_F]$ with the fast wavenumber $k_+ = k_F + \xi_+/\hbar v_F \approx k_F$, and to write the denominator in the parabolic approximation: $D_\xi(\varepsilon) \approx (\xi - \xi_+)^2 - \delta^2(\varepsilon)$, with $\delta^2(\varepsilon) = 4\Delta(\Delta + \varepsilon_0)^2 (\varepsilon_{max} - \varepsilon)/(2c\gamma^2)$ (see Fig. 5). Thus, the interaction matrix $A_n(\varepsilon) = A_n(\varepsilon) \hat{m}_+$ only depends on the distance n between impurities, and, for ε close to ε_{max} , this dependence can be expressed as:

$$A_r(\varepsilon) \approx \sqrt{\frac{r_\varepsilon}{r}} \sin k_\varepsilon r \cos k_F r, \quad (30)$$

where the length scales both for the monotonous decay:

$$r_\varepsilon = \frac{2\pi}{k_F} \left[\frac{\varepsilon_0 \rho_F (\Delta + \varepsilon_0)}{c \delta(\varepsilon)} \right]^2,$$

and for the sine factor: $k_\varepsilon^{-1} = \hbar v_F / \delta(\varepsilon)$, are much longer than k_F^{-1} for the fast cosine. The latter fast oscillation is specific for the interactions mediated by Fermi quasiparticles (like the known RKKY mechanism), unlike the monotonous or slowly oscillating interactions between impurities in semiconductors or in bosonic systems [29].

Now calculation of $\Gamma_i(\varepsilon) = c^2 T(\varepsilon) \text{Im} B(\varepsilon)$ mainly concerns the dominant scalar part of the GE pair term:

$$B(\varepsilon) \approx \frac{2\pi}{a^2} \int_a^{r_\varepsilon} \frac{r dr}{1 - 4A_r^2(\varepsilon)}, \quad (31)$$

(since the k -dependent term in Eq. (18) turns to be negligible beside this). The upper integration limit in Eq. (31) refers to the fact that its integrand only has poles for $r < r_\varepsilon$. With respect to the slow and fast modes in the function, Eq. (30), the integration is naturally divided in two stages. At the first stage, integration over each m -th period of fast cosine, around $r_m = 2\pi m / k_F$, is done setting the slow factors, $r \approx r_m$ and $\sin k_\varepsilon r \approx \sin k_\varepsilon r_m$ constant, and using the explicit formula:

$$\text{Im} \int_{-\pi}^{\pi} \frac{dx}{1 - 4A^2 \cos^2 x} = \text{Im} \frac{\pi}{\sqrt{1 - A^2}}.$$

At next stage, summation of these results in m is approximated by integration in slow variable:

$$\frac{\pi}{k_F} \text{Im} \sum_m \frac{r_m^{3/2}}{\sqrt{r_m - r_\varepsilon \sin^2 k_\varepsilon r_m}} \approx \text{Im} \int_a^{r_\varepsilon} \frac{r^{3/2}}{\sqrt{r - r_\varepsilon \sin^2 k_\varepsilon r}}. \quad (32)$$

Numerical calculation of the latter integral results in:

$$\text{Im} B = \frac{r_\varepsilon^2}{a^2} f(k_\varepsilon r_\varepsilon), \quad (33)$$

where the function $f(z)$ is zero for $z < z_0 \approx 1.3585$, and monotonously grows for $z > z_0$, rapidly reaching the asymptotic constant value: $f_{as} \approx 1.1478$, for $z \gg z_0$. Then the IRM criterion, Eq. (28), at ε so close to ε_{max} that $k_\varepsilon r_\varepsilon \gg z_0$ is expressed as:

$$\varepsilon_{max} - \varepsilon \gg \frac{c\gamma^2}{\varepsilon_{max} - \varepsilon_0} \frac{r_\varepsilon^2}{a^2}, \quad (34)$$

giving an (c -independent) estimate for the range of extended states within the impurity band:

$$\varepsilon_{max} - \varepsilon \gg \Gamma_0 = \frac{(v\varepsilon_0)^{3/2}}{ak_F} \sqrt{\frac{2\pi\rho_F}{1+v^2}}. \quad (35)$$

Its comparison with the full extension of this band, $\varepsilon_{max} - \varepsilon_{min} = c\gamma^2(1+v^2)/(v^2\Delta)$, would suggest a possibility for such extended states to really exist if the impurity concentration surpasses the characteristic (small) value:

$$c \gg c_0 = \frac{(\pi\rho_F\varepsilon_0)^{3/2}}{ak_F} \sqrt{\frac{2v}{1+v^2}}. \quad (36)$$

For typical values of $\rho_F^{-1} \sim 2$ eV, $ak_F \sim 1$, and $\Delta \sim 10$ meV in LaOFeAs system [8, 13, 58], and supposing a plausible impurity perturbation $v \sim 1$, we estimate $c_0 \approx 8 \cdot 10^{-4}$, manifesting important impurity effects already at their very low content.

However, the r. h. s. of Eq. (33) vanishes at $k_\varepsilon r_\varepsilon < z_0$, which occurs beyond the vicinity of the band top:

$$\varepsilon_{max} - \varepsilon > \left(\frac{c_0}{c}\right)^3 \Gamma_0. \quad (37)$$

Under the condition of Eq. (36), this vicinity is yet narrower than Γ_0 by Eq. (35), defining the true, even wider, range of extended states within the impurity band.

Otherwise, for $c \ll c_0$, the impurity band does not exist at all, then we analyze the energy range near the impurity level with the NRF GE and write an approximate criterion for its convergence as $c|B^0| \ll 1$. This calculation is done in a similar way to as before but replacing the interaction function, Eq. (29), by its NRF version:

$$A_r^0(\varepsilon) \approx \sqrt{\frac{R_\varepsilon}{r}} e^{-r/r_0} \cos k_F r, \quad (38)$$

with $k_F R_\varepsilon = 2\pi(\varepsilon_0/|\varepsilon - \varepsilon_0|)^2$ and $k_F r_0 = 2\varepsilon_F/\xi_0$. Then the above GE convergence criterion is assured beyond the following vicinity of impurity level:

$$|\varepsilon - \varepsilon_0| \gg \Gamma_0 \exp\left(-\frac{c_0^{4/3}}{c}\right), \quad (39)$$

defining its broadening due to inter-impurity interactions. Within this range, the DOS function for localized states can be only estimated by the order of magnitude, but outside it is given by:

$$\begin{aligned} \rho_{loc}(\varepsilon) &\approx \frac{c^2}{c_0^{4/3}} |\varepsilon - \varepsilon_0|, \quad \text{for } \Gamma_c \ll |\varepsilon - \varepsilon_0| \ll \Gamma_0, \\ \rho_{loc}(\varepsilon) &\approx \frac{c^2 \varepsilon_0^4}{|\varepsilon - \varepsilon_0|^5}, \quad \text{for } \Gamma_0 \ll |\varepsilon - \varepsilon_0|, \end{aligned} \quad (40)$$

Notably, the total number of states near the impurity level is

$$\int \rho_{loc}(\varepsilon) d\varepsilon \sim c,$$

alike that of extended states in the impurity band by Eq. (26). The summary of evolution of this area of quasiparticle spectrum in function of impurity concentration is shown in Fig. 7.

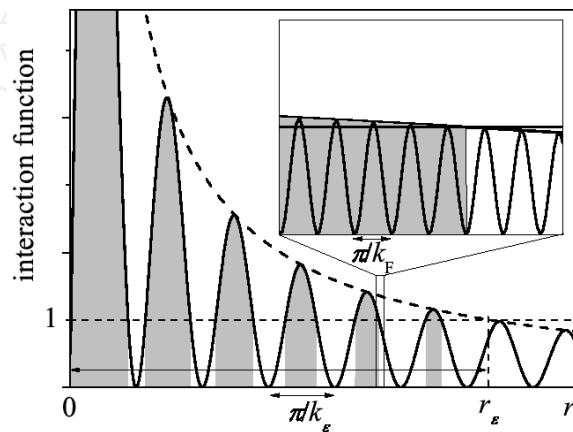


Figure 6. Interaction function $A^2_r(\varepsilon)$ by Eq. 29 at the choice of parameters $\varepsilon_{max} - \varepsilon = 0.1$ and $\Delta/\varepsilon_F = 5 \cdot 10^{-2}$ displays slower sine oscillations (solid line) and the monotonous envelope function (dashed line). The shadowed intervals are those contributing to $\text{Im } B$, accordingly to the condition $(r_\varepsilon/r)\sin^2 k_\varepsilon r > 1$. Inset: the expansion of the rectangle in the main panel shows also faster oscillations by the cosine.

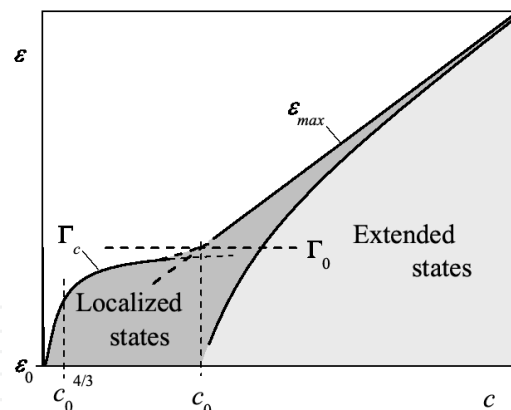


Figure 7. Composition of the energy spectrum near the impurity level ε_0 in function of impurity concentration.

5. Impurity effects on superconducting characteristics

The above results on the quasiparticle spectrum in the disordered SC system can be immediately used for calculation of impurity effects on its observable characteristics. Thus the fundamental SC order parameter Δ is estimated from the modified gap equation:

$$\lambda^{-1} = \int_0^{\varepsilon_D} \text{Im Tr } \hat{G}(\varepsilon) \hat{\tau}_1 d\varepsilon, \quad (41)$$

where $\hat{G}(\varepsilon) = N^{-1} \sum_k \hat{G}_k(\varepsilon)$, $\lambda = \rho_F V_{SC}$ is the (small) dimensionless SC pairing constant, and the Debye energy ε_D restricts the energy range of its action. In absence of impurities, $c = 0$, using of Eq. (11) leads straightforwardly to the known result for the non-perturbed Δ_0 value: $\lambda^{-1} = \text{arccosh}(\varepsilon_D/\Delta_0)$ and thus $\Delta_0 \approx 2\varepsilon_D e^{-1/\lambda}$.

For finite c , contributions to Eq. (41) come both from the main band, Eq. (25), and from the impurity band (or level), Eqs. (26) (or (40)). The latter contribution is $\sim c$, accordingly to the previous discussion, defining a small correction beside $\lambda^{-1} \gg 1$. But a much stronger c -dependent correction comes from the modified main band (limited to its range of extended states):

$$\int_{\varepsilon_c}^{\varepsilon_D} \frac{d\varepsilon}{\sqrt{\varepsilon^2 - \Delta^2}} = \text{arccosh} \frac{\varepsilon_D}{\Delta} - \text{arccosh} \frac{\varepsilon_c}{\Delta}.$$

For $\varepsilon_c - \Delta \sim (c/c_1)^2 \Delta$ (see after Eq. (24)) and $c \ll c_1$, the last term is well approximated by:

$$\text{arccosh} \frac{\varepsilon_c}{\Delta} \approx \sqrt{2} \frac{c}{c_1},$$

and leads to the modified gap equation as:

$$\text{arccosh} \frac{\varepsilon_D}{\Delta} - \text{arccosh} \frac{\varepsilon_D}{\Delta_0} \approx \sqrt{2} \frac{c}{c_1}, \quad (42)$$

Its approximate solution for $c \ll c_1$ describes the initial decay of SC order parameter with impurity concentration as:

$$\Delta \approx \Delta_0 \left(1 - \sqrt{2} \frac{c}{c_1} \right), \quad (43)$$

and for the values of ρ_F and Δ_0 used above, the estimate of characteristic concentration c_1 is quite low: $c_1 \sim 10^{-2}$ (though higher than c_0 by Eq. (36)), suggesting a very strong impurity effect. With further growing c up to $c < c_1$, the value of Δ from Eq. (43) would formally tend to zero as $\approx \Delta_0 (c_1/c)^2/2$. However, concentrations $c \sim c_1$ would already correspond to the impurity band as wide as the gap itself; this goes beyond the validity of the present approach and needs a special treatment.

To study another important dependence, that of the SC transition temperature T_c on concentration c , one has, strictly speaking, to extend the above GF techniques for finite temperatures, but a very simple estimate can be done, supposing that the BCS relation $\Delta/T_c \approx 1.76$ still holds in the presence of impurities. Then the r.h.s. of Eq. (44) would also describe the decay of T_c/T_{c0} .

It is of interest to compare the present results with the known Abrikosov-Gor'kov solution for BCS SC with paramagnetic impurities in the Born approximation [59, 60]. In that approximation, the only perturbation parameter is the (constant) quasiparticle lifetime τ . In our framework, τ^{-1} can be related to $\text{Im } \Sigma(\varepsilon)$ at a proper choice of energy, $\varepsilon \sim |\Delta - \varepsilon| \sim \Delta$. Then, in the self-consistent T-matrix approximation [cite{psl}], we estimate $\tau^{-1} \sim c\Delta/c_1$ which leads to the relation $\tau T_c \sim c_1/(1.76c)$, reaching at $c \sim c_1$ a good agreement with the Abrikosov-Gor'kov universal criterion for complete SC suppression $\tau T_c < 0.567$.

Also, a notable impurity effect is expected on the London penetration depth $\lambda_L \sim n_s^{-1/2}$, as follows from the temperature dependence of superfluid density:

$$n_s(T) = \int_0^\infty \frac{\rho(\varepsilon) d\varepsilon}{e^{\varepsilon/k_B T} + 1} \approx n_s^0(T) - \frac{cv^2}{1+v^2} \frac{\Delta}{\varepsilon_F} \sqrt{\frac{k_B T}{\pi\Delta}} e^{-\Delta/k_B T} + \frac{c}{e^{\varepsilon_0/k_B T} + 1}. \quad (44)$$

When compared to its unperturbed value in the pure SC system

$$n_s^0(T) = \rho_F \int_\Delta^\infty \frac{\varepsilon d\varepsilon}{(e^{\varepsilon/k_B T} + 1) \sqrt{\varepsilon^2 - \Delta^2}} \approx c_1 \sqrt{\frac{k_B T}{2\pi\Delta}} e^{-\Delta/k_B T},$$

the effect by the last term in Eq. (45) produces a considerable slowing down of the low-temperature decay of the difference $\lambda(T)/\lambda(0) - 1$ (Fig. 8), in a reasonable agreement with recent experimental observations for SC iron pnictides under doping [47].

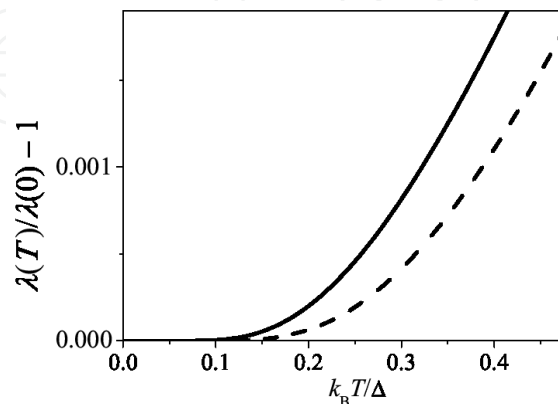


Figure 8. Low-temperature decay of the London penetration depth difference for a SC with impurities (solid line) is slower than that in absence of impurities (dashed line).

Finally, a similar analysis can be applied for the impurity effect on the electronic specific heat in the SC state, whose dependence on inverse temperature $\beta = 1/(k_B T)$ is represented as:

$$C(\beta) = \frac{\partial}{\partial \beta} \int_0^\infty \frac{\varepsilon \rho(\varepsilon) d\varepsilon}{e^{\beta \varepsilon} + 1}, \tag{45}$$

and naturally divided in two characteristic contributions, $C = C_i + C_b$, from ρ_i and ρ_b states:

$$C_i(\beta) \approx ck_B \left[\frac{\beta \varepsilon_0}{2 \cosh(\beta \varepsilon_0 / 2)} \right]^2,$$

$$C_b(\beta) \approx k_B (c_1 - c) v(\beta \Delta)^{3/2} \exp(-\beta \Delta).$$

The resulting function $C(\beta)$ deviates from the known low temperature behavior $C_0(\beta) \sim \exp(-\beta \Delta)$ for non-perturbed SC system at $\beta > \ln(c_1/c - 1)/(\Delta - \varepsilon_0)$, where the characteristic exponent is changed to a slower $\sim \exp(-\beta \varepsilon_0)$ as seen in Fig. 9.

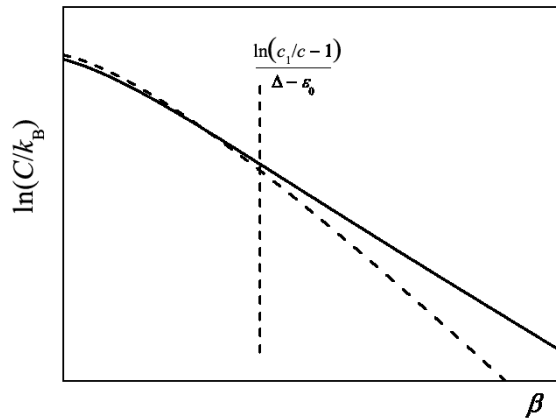


Figure 9. Temperature behavior of specific heat for a SC with impurities presents a crossover from $\beta \Delta$ exponent (dashed line) to $\beta \varepsilon_0$ at low enough temperature (high enough $\beta = 1/(k_B T)$).

The same approach can be then used for other observable characteristics for SC under impurity effect, such as, e.g., heat conductivity, differential conductivity for scanning tunneling spectroscopy or absorption coefficient for far infrared radiation that is done in the next section.

6. Kubo-Greenwood formalism for multiband superconductor

The relevant kinetic coefficients for electronic processes in the considered disordered superconductor follow from the general Kubo-Greenwood formulation [55, 56], adapted here to the

specific multiband structure of Green function matrices. Thus, one of the basic transport characteristics, the (frequency and temperature dependent) electrical conductivity is expressed in this approach as:

$$\sigma(\omega, T) = \frac{e^2}{\pi} \int d\varepsilon \frac{f(\varepsilon) - f(\varepsilon')}{\omega} \int d\mathbf{k} v_x(\mathbf{k}, \varepsilon) v_x(\mathbf{k}, \varepsilon') \text{Tr} \left[\text{Im} \hat{G}_k(\varepsilon) \text{Im} \hat{G}_k(\varepsilon') \right], \quad (46)$$

for $\varepsilon' = \varepsilon - \hbar\omega$ and the electric field applied along the x -axis. Besides the common Fermi occupation function $f(\varepsilon) = (e^{\beta\varepsilon} + 1)^{-1}$, the above formula involves the generalized velocity function:

$$v(\mathbf{k}, \varepsilon) = \left(\hbar \frac{\partial \text{Re} D_k(\varepsilon)}{\partial \varepsilon} \right)^{-1} \nabla_k \text{Re} D_k(\varepsilon). \quad (47)$$

This function is defined in the whole ξ, ε plane in a way to coincide with the physical quasi-particle velocities for each particular band, Eqs. (23, 24), along the corresponding dispersion laws: $v(\mathbf{k}, \varepsilon_j(\mathbf{k})) = \hbar^{-1} \nabla_k \varepsilon_j(\mathbf{k}) = v_{j, \nu} \quad j = b, i$. The conductivity resulting from Eq. (48) can be then used for calculation of optical reflectivity.

Other relevant quantities are the static (but temperature dependent) transport coefficients, as the heat conductivity:

$$\kappa(T) = \frac{\hbar}{\pi} \int d\varepsilon \frac{\partial f(\varepsilon)}{\partial \varepsilon} \int d\mathbf{k} [v_x(\mathbf{k}, \varepsilon)]^2 \text{Tr} \left[\text{Im} \hat{G}_k(\varepsilon) \right]^2, \quad (48)$$

and the thermoelectric coefficients associated with the static electrical conductivity $\sigma(T) \equiv \sigma(0, T)$ [62], the Peltier coefficient:

$$\Pi(T) = \frac{\hbar e}{\pi \sigma(T)} \int d\varepsilon \frac{\partial f(\varepsilon)}{\partial \varepsilon} \varepsilon \int d\mathbf{k} [v_x(\mathbf{k}, \varepsilon)]^2 \text{Tr} \left[\text{Im} \hat{G}_k(\varepsilon) \right]^2, \quad (49)$$

and the Seebeck coefficient $S(T) = \Pi(T)/T$. All these transport characteristics, though being relatively more complicated from the theoretical point of view than the purely thermodynamical quantities from the previous section, permit an easier and more reliable experimental verification and so could be of higher interest for practical applications of the considered impurity effects in the multiband superconductors.

It is worth to recall that the above formulae are only contributed by the band-like states, that is the energy arguments $\varepsilon, \varepsilon'$ in Eqs. (47, 49, 50) are delimited by the relevant mobility edges.

This is the main distinction of our approach from the existing treatments of impurity effects on transport in iron pnictide superconductors using the T-matrix approximation to a solution like Eq. (15) for the whole energy spectrum [62], even for its ranges where the very concept of velocity, as Eq. (48), ceases to be valid.

Next, we consider the particular calculation algorithms for the expressions, Eqs. (47, 49, 50), for the more involved case of dynamical conductivity, Eq. (47), that can be then reduced to simpler static quantities, Eqs. (49, 50).

7. Optical conductivity

The integral in Eq. (47) is dominated by the contributions from δ -like peaks of the $\text{Im } \hat{G}_k(\varepsilon)$ and $\text{Im } G_k(\varepsilon')$ matrix elements. These peaks arise from the above dispersion laws, Eqs. (23), (24), thus restricting the energy integration to the band-like ranges: $|\varepsilon| > \varepsilon_c$ for the b -bands and $\varepsilon_{c,-} < |\varepsilon| < \varepsilon_{c,+}$ for the i -bands. Regarding the occupation numbers $f(\varepsilon)$ and $f(\varepsilon')$ at reasonably low temperatures $k_B T \ll \Delta, \varepsilon_0$, the most effective contributions correspond to positive ε values, either from b - or i -bands, and to negative ε' values from their negative counterparts, b' or i' . There are three general kinds of such contributions: i) b - b' , due to transitions between the main bands, similar to those in optical conductivity by the pure crystal (but with a slightly shifted frequency threshold: $\hbar\omega \sim 2\varepsilon_c$), ii) b - i' (or i - b'), due to combined transitions between the principal and impurity bands within the frequency range $\hbar\omega \sim \varepsilon_c + \varepsilon_{c,-}$ and iii) i - i' , due to transitions between the impurity bands within a narrow frequency range of $2\varepsilon_{c,-} < \hbar\omega < 2\varepsilon_{c,+}$. The frequency-momentum relations for these processes and corresponding peaks are displayed in Fig. 10. The resulting optical conductivity reads $\sigma(\omega, T) = \sum_{\alpha} \sigma_{\alpha}(\omega, T)$ with $\alpha = b$ - b' , i - i' , and i - b' .

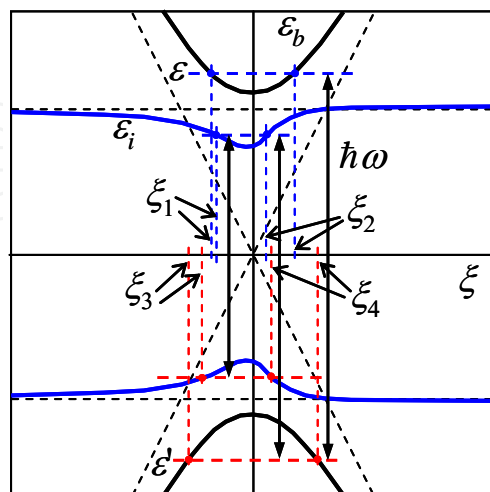


Figure 10. Configuration of the poles ξ_j of GF's contributing to different types of optical conductivity processes (over electronic pocket of the quasiparticle spectrum in Fig. 3).

For practical calculation of each contribution, the relevant matrix $\text{Im } \hat{G}_k(\varepsilon)$ (within the band-like energy ranges) can be presented as $\text{Im } \hat{G}_k(\varepsilon) = \hat{N}(\varepsilon, \xi) \text{Im} [D_k(\varepsilon)^{-1}]$ where the numerator matrix:

$$\hat{N}(\varepsilon, \xi) = \text{Re} (\tilde{\varepsilon} + \tilde{\xi}\tau_3 + \Delta\tau_1), \quad (50)$$

is a smooth enough function while the above referred peaks result from zeros of $\text{Re } D_k(\varepsilon)$. Now, the quasimomentum integration in Eq. (47) under the above chosen symmetry of Fermi segments spells as $\int d\varphi \int dk = 2(hv_F)^{-1} \int d\varphi \int d\xi$ where the factor 2 accounts for identical contributions from e - and h -segments. The azimuthal φ -integration contributes by the factor of π (from x -projections of velocities) and the most important radial ξ -integration is readily done after expanding its integrand in particular pole terms:

$$v(\xi, \varepsilon)v(\xi, \varepsilon') \text{Tr} [\text{Im } \hat{G}(\xi, \varepsilon)\text{Im } \hat{G}(\xi, \varepsilon')] = \sum_{\alpha} A_{\alpha}(\varepsilon, \varepsilon')\delta(\xi - \xi_{\alpha}), \quad (51)$$

where $v(\xi, \varepsilon) = |v_k(\varepsilon)|$ and $\hat{G}(\xi, \varepsilon) \equiv \hat{G}_k(\varepsilon)$ define the respective residues:

$$A_{\alpha}(\varepsilon, \varepsilon') = \pi v_{\alpha} v'_{\alpha} \frac{\tilde{\varepsilon}\tilde{\varepsilon}' + \tilde{\xi}\tilde{\xi}' + \Delta^2}{\prod_{\beta \neq \alpha} (\xi_{\alpha} - \xi_{\beta})}. \quad (52)$$

Here $v_{\alpha} \equiv v(\varepsilon, \xi_{\alpha})$, $v'_{\alpha} \equiv v(\varepsilon', \xi_{\alpha})$, and the indices α, β run over all the poles of the two Green functions. As seen from Eqs. (23, 24) and Fig. 10, there can be two such poles of $\hat{G}(\xi, \varepsilon)$ related to band-like states with positive ε and respective quasi-momentum values denoted as $\xi_{1,2}(\varepsilon)$. For energies within the b -band, $\varepsilon > \varepsilon_c$, they are symmetrical:

$$\xi_{1,2}(\varepsilon) \approx \pm \sqrt{\varepsilon^2 - \Delta^2}, \quad (53)$$

but within the i -band, at $\varepsilon_{c,-} < |\varepsilon| < \varepsilon_{c,+}$ their positions are asymmetrical:

$$\xi_{1,2}(\varepsilon) \approx \frac{c\gamma^2 \mp 2\varepsilon_0 \sqrt{(\varepsilon_+ - \varepsilon)(\varepsilon - \varepsilon_-)}}{2(\varepsilon - \varepsilon_0)}. \quad (54)$$

Within the i -band, there is a narrow vicinity of ε_0 of $\sim c_0^{1/3}(c_0/c)^3\varepsilon_0$ width where only the ξ_1 pole by Eq. (54) is meaningful and the other contradicts the IRM criterion (so that there is no band-like states with those formal ξ_2 values in this energy range). Analogous poles of $\hat{G}(\xi, \varepsilon')$ at negative ε' are referred to as $\xi_{3,4}(\varepsilon')$ in what follows. Taking into account a non-zero $\text{Im } D_k(\varepsilon)$ (for the i -band, it is due to the non-trivial terms in the group expansion, Eq. (16)), each α -th pole becomes a δ -like peak with an effective linewidth Γ_{α} but this value turns to be essential only at calculation of static coefficients like Eqs. (49, 50).

Since four peaks in Eq. (47) are well separated, the ξ -integration is done considering them true δ -functions, then the particular terms in $\sigma(\omega, T)$ are given by the energy integrals:

$$\sigma_\nu(\omega, T) = 2e^2 \int_{\varepsilon_{\nu,-}}^{\varepsilon_{\nu,+}} d\varepsilon \frac{f(\varepsilon) - f(\varepsilon')}{\omega} \sum_{\alpha=1}^4 A_{\alpha'} \tag{55}$$

for $\nu = b-b', i-b'$, or $i-i'$ and the limits $\varepsilon_{\nu,\pm}$ should assure both ε and ε' to be within the band-like ranges. Thus, in the $b-b'$ term, the symmetry of the poles $\xi_{1,2}(\varepsilon)$ and $\xi_{1,2}(\varepsilon')$ by Eq. (55) and the symmetry of b - and b' -bands themselves defines their equal contributions, then using simplicity of the function $v(\varepsilon, \xi) = \xi/\varepsilon$ and non-renormalized energy $\tilde{\varepsilon} \rightarrow \varepsilon$ and momentum $\xi \rightarrow \xi$, integration between $\varepsilon_{b-b',-} = \varepsilon_c$ and $\varepsilon_{b-b',+} = \hbar\omega - \varepsilon_c$ gives an analytic form $\sigma_{b-b'}(\omega, T) = \sigma_{b-b'}(\omega, 0) - \sigma_{b-b',T}(\omega)$. Here the zero-temperature limit value is:

$$\sigma_{b-b'}(\omega, 0) \approx \sigma_0 \frac{2\omega_c}{\omega^2} \left\{ \sqrt{4\omega^2 - \omega_c^2} \ln \left[2 \frac{\omega(2\omega - \omega_c) + \sqrt{\omega(\omega - \omega_c)(4\omega^2 - \omega_c^2)}}{\omega_c^2} - 1 \right] + 2\omega \ln \left[2 \frac{\omega - \sqrt{\omega(\omega - \omega_c)}}{\omega_c} - 1 \right] - 2\sqrt{\omega(\omega - \omega_c)} \right\}, \tag{56}$$

with characteristic scale $\sigma_0 = e^2/\Delta^2$ and simple asymptotics:

$$\sigma_{b-b'}(\omega, 0) \approx \sigma_0 \begin{cases} \frac{2}{3} \left(\frac{\omega}{\omega_c} - 1 \right)^{3/2}, & \omega - \omega_c \ll \omega_c, \\ \frac{32\omega_c}{\omega} \ln \frac{2\omega}{\omega_c}, & \omega \gg \omega_c, \end{cases}$$

vs the threshold frequency $\omega_c = 2\varepsilon_c/\hbar$, reaching the maximum value $\approx 1.19\sigma_0$ at $\omega \approx 2.12 \omega_c$ (Fig. 11). The (small) finite-temperature correction to Eq. (57) is:

$$\sigma_{b-b',T}(\omega) \approx \sigma_0 \frac{2\omega_c^2 e^{-\beta\Delta}}{\beta\omega(\omega - \omega_c)\sqrt{\Delta}} \left\{ \frac{\sqrt{\hbar\omega}}{\Delta} \left[1 - \frac{F(\sqrt{\beta\hbar(\omega - \omega_c)})}{\sqrt{\beta\hbar(\omega - \omega_c)}} \right] + \frac{\sqrt{2\Delta}}{\hbar\omega - \Delta} \left[\frac{\sqrt{\pi}}{2} \frac{\text{erf}(\sqrt{\beta\hbar(\omega - \omega_c)})}{\sqrt{\beta\hbar(\omega - \omega_c)}} - e^{-\beta\hbar(\omega - \omega_c)} \right] \right\}, \tag{57}$$

with the Dawson function $F(z) = \sqrt{\pi}e^{-z^2}\text{erf}(iz)/(2i)$ and the error function $\text{erf}(z)$ [64].

Calculation of the i - b' -term is more complicated since asymmetry of the i -band poles $\xi_{1,2}(\varepsilon)$ by Eq. (55) and their non-equivalence to the symmetric poles $\xi_{3,4}(\varepsilon')$ of the b' -band analogous to Eq. (54). Also the generalized velocity function within the i -band range:

$$\hbar v(\xi, \varepsilon) = \frac{c\gamma^2 - \xi(\varepsilon - \varepsilon_0)}{\varepsilon(\varepsilon - \varepsilon_0 - c\gamma^2 / \varepsilon_0)}, \quad (58)$$

and the energy integration limits: $\varepsilon'_{i-b,-} = \varepsilon_{c,-}$ and $\varepsilon'_{i-b,+} = \min[\varepsilon_{c,+}, \hbar\omega - \varepsilon_c]$ are more complicated. Then $\sigma_{i-b}(\omega, T)$ follows from numerical integration in Eq. (56); as seen in Fig. 11, it has a lower threshold frequency $\omega_c = \varepsilon_c + \varepsilon_{c,-}$ than the b - b' -term. Above this threshold, it grows linearly as $\sim (\omega/\omega_c - 1)c^{5/2}c_0^{-5/3}\sigma_0$ and, for "safe" impurity concentrations $c \ll c_1 \sim c_0^{2/3}$, becomes fully dominated by the b - b' term, Eq. (57) above its threshold ω_c . Finally, the i - i' -term from a similar numerical routine on Eq. (56) within integration limits $\varepsilon_{i-i,-} = \varepsilon_{c,-}$ and $\varepsilon_{i-i,+} = \min[\varepsilon_{c,+}, \hbar\omega - \varepsilon_{c,-}]$, using Eq. (55) for the poles $\xi_{1,2}(\varepsilon)$ and $\xi_{3,4}(\varepsilon')$ and Eq. (59) for generalized velocities. The resulting $\sigma_{i-i'}(\omega, T)$ occupies a narrow frequency band from $\omega_{i-i'} = 2\varepsilon_{c,-}/\hbar$ to $\omega_{i-i',+} = 2\varepsilon_{c,+}/\hbar$ (Fig. 11) with asymptotics near these thresholds in the zero-temperature limit:

$$\sigma_{i-i'}(\omega, 0) \approx \sigma_0 \frac{16c^{7/2}\gamma^7}{3\sqrt{2}\xi_-^7} \left(\frac{\omega - \omega_-}{\omega_-} \right)^{3/2}, \quad (59)$$

at $0 < \omega - \omega_- \ll \omega_-$ and alike for $0 < \omega_+ - \omega \ll \omega_+$ with only changes: $\xi_- \rightarrow \xi_+, \omega_- \rightarrow \omega_+$.

Extrapolation of these asymptotics to the center of impurity band gives an estimate for the maximum of i - i' term: $\sigma_{i-i',max} \sim c^5c_0^{-10/3}(\xi_+/\xi_-)^{7/2}\sigma_0$. It shows that the narrow i - i' peak of optical conductivity around $\omega \approx 2\varepsilon_0/\hbar$, unlike the "combined" i - b' term, can become as intense as the "main" b - b' intensity, Eq. (58), if the small factor $\sim (c/c_1)^5$ be overweighted by the next factor $(\xi_+/\xi_-)^{7/2}$. It is only possible for weak enough impurity perturbation: $v \ll 1$. Then the ratio $\xi_+/\xi_- \approx (2/v)^2 < 1$ can really overweight the concentration factor if c reaches $\sim c_1(v/2)^{7/5} \ll c_1$, that is quite realistic within the "safety" range $c \ll 1$. The overall picture of optical conductivity for an example of weakly coupled, $v = 0.25$, impurities at high enough $c = 4c_0$ is shown in Fig. 11. The effect of "giant" optical conductivity by the in-gap impurity excitations could be compared with the known Rashba enhancement of optical luminescence by impurity levels near the edge of excitonic band [64] or with huge impurity spin resonances in magnetic crystals [29], but here it appears in a two-particle process instead of the above mentioned single-particle ones.

To emphasize, the considered impurity features in optical conductivity cannot be simply treated as optical transitions between localized impurity states (or between these and main

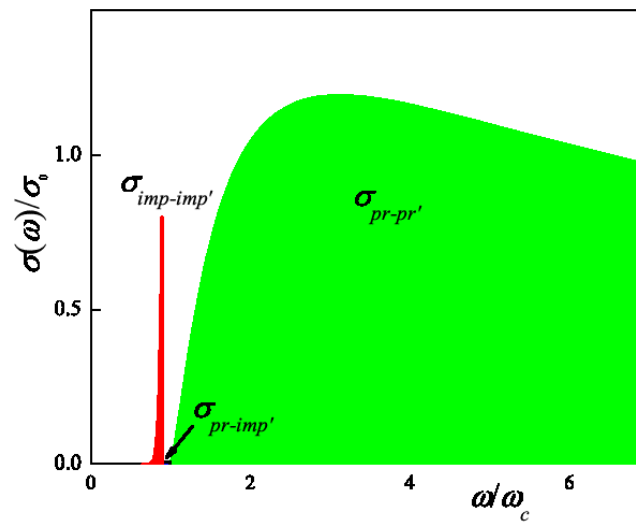


Figure 11. General picture of the optical conductivity showing three types of contributions.

bands) since localized states can not contribute to currents. Such effects only appear at high enough impurity concentrations, $c \rightarrow c_0$, when the impurity banding takes place.

8. Concluding remarks

Resuming, the GF analysis of quasiparticle spectra in SC iron pnictides with impurities of simplest (local and non-magnetic) perturbation type permits to describe formation of impurity localized levels within SC gap and, with growing impurity concentration, their evolution to specific bands of extended quasiparticle states, approximately described by quasimomentum but mainly supported by the impurity centers. Explicit dispersion laws and densities of states are obtained for the modified main bands and impurity bands. Further specification of the nature of all the states in different energy ranges within the SC gap is obtained through analysis of different types of GEs for self-energy matrix, revealing a complex oscillatory structure of indirect interactions between impurity centers and, after their proper summation, resulting in criteria for crossovers between localized and extended states. The found spectral characteristics are applied for prediction of several observable impurity effects.

Besides the thermodynamical effects, expected to appear at all impurity concentrations, that is either due to localized or band-like impurity states, a special interest is seen in the impurity effects on electronic transport in such systems, only affected by the impurity band-like states. It is shown that the latter effects can be very strongly pronounced, either for high-frequency transport and for static transport processes. In the first case, the strongest impurity effect is expected in a narrow peak of optical conductance near the edge of conductance band in non-perturbed crystal, resembling the known resonance enhancement of impurity absorption (or emission) near the edge of quasiparticle band in normal systems. The static transport coefficients at overcritical impurity concentrations are also expected to be strongly enhanced compared to those in a non-perturbed system, including the thermoelectric Peltier and Seebeck coefficients.

The proposed treatment can be adapted for more involved impurity perturbations in SC iron pnictides, including magnetic and non-local perturbations, and for more realistic multiorbital structures of the initial iron pnictide system. Despite some quantitative modifications of the results, their main qualitative features as possibility for new narrow in-gap quasiparticle bands and related sharp resonant peaks in transport coefficients should be still present. The experimental verifications of such predictions would be of evident interest, also for important practical applications, e.g., in narrow-band microwave devices or advanced low-temperature sensors, though this would impose rather hard requirements on quality and composition of the samples, to be extremely pure aside the extremely low (by common standards) and well controlled contents of specially chosen and uniformly distributed impurity centers. This can be compared to the requirements on doped semiconductor devices and hopefully should not be a real problem for modern lab technologies.

Acknowledgements

Y.G.P. and M.C.S. acknowledge the support of this work through the Portuguese FCT project PTDC/FIS/101126/2008. V.M.L. is grateful to the Special Program of Fundamental Research of NAS of Ukraine.

Parts of the chapter are reproduced from the authors' previous publication [53]

Author details

Yuriy G. Pogorelov^{1*}, Mario C. Santos² and Vadim M. Loktev³

*Address all correspondence to: ypogorel@fc.up.pt

1 IFIMUP-IN, Departamento de Física, Universidade do Porto, Porto, Portugal

2 Departamento de Física, Universidade de Coimbra, R. Larga, Coimbra, Portugal

3 Bogolyubov Institute for Theoretical Physics, NAN of Ukraine, Kiev, Ukraine

References

- [1] Kamihara Y, Hiramatsu H, Hirano M, Kawamura R, Yanagi H, Kamiya T, Hosono H. Iron-Based Layered Superconductor: LaOFeP. *J. Am. Chem. Soc.* 2006;128:10012–10013. DOI: 10.1021/ja063355c

- [2] Kamihara Y, Watanabe T, Hirano M, Hosono H. Iron-based Layered Superconductor $\text{La}[\text{O}_{1-x}\text{F}_x]\text{FeAs}$ ($x=0.05-0.12$) with $T_c = 26\text{K}$. *J. Am. Chem. Soc.* 2008;130:3296-3297. DOI: 10.1021/ja800073m
- [3] Sadovskii MV. High-temperature superconductivity in iron-based layered iron compounds. *Phys. Uspekhi.* 2008;178:1201-1227. DOI: 10.1070/PU2008v051n12ABEH006820
- [4] Izyumov YA, Kurmaev EZ. Materials with strong electron correlations. *Phys. Uspekhi.* 2008;51:23-56. DOI: 10.1070/PU2008v051n01ABEH006388
- [5] Ginsberg DM, editor. *Physical Properties of High Temperature Superconductors I.* World Scientific;1989. 509 p. ISBN: 9971-50-683-1 9971-50-894-X(pbk)
- [6] Takahashi H, Igawa K, Arii K, Kamihara Y, Hirano M, Hosono H. Superconductivity at 43K in an iron-based layered compound $\text{LaO}_{1-x}\text{F}_x\text{FeAs}$. *Nature* 2008;453:376-378. DOI: 10.1038/nature06972
- [7] Norman MR. High-temperature superconductivity in the iron-pnictides. *Physics* 2008;1: 21-26. DOI: 10.1103/Physics.1.21.6
- [8] Ding H, Richard P, Nakayama K, Sugawara K, Arakane T, Sekiba Y, Takayama A, Souma T, Takahashi T, Wang Z, Dai X, Fang Z, Chen GF, Luo JL, Wang NL. Observation of Fermi-surface-dependent nodeless superconducting gaps in $\text{Ba}_{0.6}\text{K}_{0.4}\text{Fe}_2\text{As}_2$. *Europhysics Lett.* 2008;83:47001. DOI: 10.1209/0295-5075/83/47001
- [9] Kondo T, Santander-Syro AF, Copie O, Liu C, Tillman ME, Mun ED, Schmalian J, Bud'ko SL, Tanatar MA, Canfield PC, Kaminski A. Momentum Dependence of the Superconducting Gap in $\text{NdFeAsO}_{0.9}\text{F}_{0.1}$. *Phys. Rev. Lett.* 2008;101:147003. DOI: <http://dx.doi.org/10.1103/PhysRevLett.101.147003>
- [10] Mazin II, Singh DJ, Johannes MD, Du MH. Unconventional Superconductivity with a Sign Reversal in the Order Parameter of $\text{LaFeAsO}_{1-x}\text{F}_x$. *Phys. Rev. Lett.* 2008;101:057003. DOI: <http://dx.doi.org/10.1103/PhysRevLett101.057003>
- [11] Luetkens H, Klauss HH, Kraken M, Litterst FJ, Dellmann T, Klingeler R, Hess C, Khasanov R, Amato A, Baines C, Kosmala M, Schumann OJ, Braden M, Hamann-Borrero J, Leps N, Kondrat A, Behr G, Werner J, Buechner B. The electronic phase diagram of the $\text{LaO}_{1-x}\text{F}_x\text{FeAs}$ superconductor. *Nature Materials Lett.* 2008; DOI: 10.1038/nmat2397
- [12] Singh DJ, Du MH. Density Functional Study of $\text{LaFeAsO}_{1-x}\text{F}_x$: A Low Carrier Density Superconductor Near Itinerant Magnetism. *Phys. Rev. Lett.* 2008;100:237003. DOI: <http://dx.doi.org/10.1103/PhysRevLett100.237003>
- [13] Haule K, Shim JH, Kotliar G, Correlated Electronic Structure of $\text{LaO}_{1-x}\text{F}_x\text{FeAs}$. *Phys. Rev. Lett.* 2008;100:226402. DOI: <http://dx.doi.org/10.1103/PhysRevLett100.226402>

- [14] Xu G, Ming W, Yao Y, Dai X, Zhang SC, Fang Z. Doping-dependent phase diagram of LaOMAs (M=V-Cu) and electron-type superconductivity near ferromagnetic instability. *et al*, Europhys Lett. 2008;82 :67002. DOI : 10.1209/0295-5075/82/67002
- [15] Raghu S, Qi XL, Liu CX, Scalapino DJ, Zhang SC. Minimal two-band model of superconducting iron oxypnictides. Phys. Rev. B 2008;77:220503. DOI: <http://dx.doi.org/10.1103/PhysRevB.77.220503>
- [16] Kuroki K, Onari S, Arita R, Usui H, Tanaka Y, Kontani H, Aoki H. Unconventional Pairing Originating from the Disconnected Fermi Surfaces of Superconducting La-FeAsO_{1-x}F_x. Phys. Rev. Lett. 2008;101:087004. DOI: <http://dx.doi.org/10.1103/PhysRevLett.101.087004>
- [17] Boeri L, Dolgov OV, Golubov AA. Is LaFeAsO_{1-x}F_x an Electron-Phonon Superconductor ? Phys. Rev. Lett. 2008;101:026403. DOI: <http://dx.doi.org/10.1103/PhysRevLett.101.026403>
- [18] Gao Y. Interorbital Pairing and its Physical Consequences in Iron Pnictide Superconductors. Phys. Rev. B 2010;81:104504. DOI: 10.1103/PhysRevB.81.104504
- [19] Si Q, Abrahams E. Strong correlations and magnetic frustration in the high T_c iron pnictides. Phys. Rev. Lett. 2008;101:076401. DOI: <http://dx.doi.org/10.1103/PhysRevLett.101.076401>
- [20] Daghofer M, Moreo A, Riera JA, Arrigoni E, Scalapino DJ, Dagotto E. Model for the Magnetic Order and Pairing Channels in Fe Pnictide Superconductors. Phys. Rev. Lett. 2008;101:237004. DOI: <http://dx.doi.org/10.1103/PhysRevLett.101.237004>
- [21] Tsai WF, Zhang YY, Fang C, Hu JP. Impurity-induced bound states in iron-based superconductors with s-wave cos k_x cos k_y pairing symmetry. Phys. Rev. B 2009;80:064513. DOI: <http://dx.doi.org/10.1103/PhysRevB.80.064513>
- [22] Graser S, Maier TA, Hirschfeld PJ, Scalapino DJ. Near-degeneracy of several pairing channels in multiorbital models for the Fe pnictides. New J. Phys. 2009 ;11:025016. DOI: 10.1088/1367-2630/11/2/025016
- [23] Maier TA, Graser S, Scalapino DJ, Hirschfeld PJ. Origin of gap anisotropy in spin fluctuation models of the iron pnictides. Phys. Rev. B 2009;79:224510. DOI: <http://dx.doi.org/10.1103/PhysRevB.79.224510>
- [24] Zhang D. Nonmagnetic Impurity Resonances as a Signature of Sign-Reversal Pairing in FeAs-Based Superconductors. Phys. Rev. Lett. 2009;103:186402. DOI: <http://dx.doi.org/10.1103/PhysRevLett.103.186402>
- [25] Zhang YY, Fang C, Zhou X, Seo K, Tsai WF, Bernevig BA, Hu J. Quasiparticle scattering interference in superconducting iron pnictides. Phys. Rev. B 2009;80:094528. DOI: <http://dx.doi.org/10.1103/PhysRevB.80.094528>

- [26] Anderson PW. Theory of dirty superconductors. *J. Phys. Chem. Solids* 1959;11:26-30. DOI: 10.1016/0022-3697(59)90036-8
- [27] Shklovskii BI, Efros AL. *Electronic properties of doped semiconductors*, Springer-Verlag, 1984, 387 p. DOI: 10.1007/978-3-662-02403-4
- [28] Ivanov MA, Pogorelov YG, *Electron Properties of Two-Parameter Long-Range Impurity States*. *Sov. Phys. JETP* 1985;61:1033-1039. DOI: 10.1134/0038-5646/85/051033-07
- [29] Ivanov MA, Loktev VM, Pogorelov YG, *Long-range impurity states in magnetic crystals*. *Phys. Reports* 1987;153:209-330. DOI: 10.1016/0370-1573(87)90103-7
- [30] Yamamoto H, Fang ZQ, Look DC. Nonalloyed ohmic contacts on low-temperature molecular beam epitaxial GaAs: Influence of deep donor band. *Appl. Phys. Lett.* 1990;57:1537-1539. DOI: <http://dx.doi.org/10.1063/1.103345>
- [31] Anderson PW. Absence of Diffusion in Certain Random Lattices. *Phys. Rev.* 1958;109:1492-1505. DOI: <http://dx.doi.org/10.1103/PhysRev.109.1492>
- [32] Mott NF. Electrons in disordered structures. *Adv. Phys.* 1967;16:49-144. DOI: 10.1080/00018736700101265
- [33] Ioffe AF, Regel AR. Non-crystalline, amorphous and liquid electronic semiconductors. *Prog. Semicond.* 1960;4:237-291.
- [34] Shiba H. Classical Spins in Superconductors. *Prog. Theor. Phys.* 1968;40:435-451. DOI: 10.1143/PTP.40.435
- [35] Rusinov AI. On the Theory of Gapless Superconductivity in Alloys Containing Paramagnetic Impurities. *Sov. Phys. JETP* 1969;29:1101-1106. DOI: 10.1134/0038-5646/69/061101-06
- [36] Maki K. Anomalous Scattering by Magnetic Impurities in Superconductors. *Phys. Rev.* 1967;153:428-434. DOI: <http://dx.doi.org/10.1103/PhysRev.153.428>
- [37] Gonnelli RS, Daghero D, Ummerino, Calzolari A, Tortello M, Stepanov VA, Zhigadlo ND, Rogacki K, Karpinski J, Bernardini F, Massidda S. Effect of Magnetic Impurities in a Two-Band Superconductor : A Point-Contact Study of Mn-Substituted MgB₂ Single Crystals. *Phys. Rev. Lett.* 2006;97:037001. DOI: <http://dx.doi.org/10.1103/PhysRevLett.97.037001>
- [38] Moca CP, Demler E, Janko B, Zarand G. Spin-resolved spectra of Shiba multiplets from Mn impurities in MgB₂. *Phys. Rev. B* 2008;77:174516. DOI: <http://dx.doi.org/10.1103/PhysRevB.77.174516>
- [39] Balatsky AV, Salkola MI, Rosengren A. Impurity-induced virtual bound states in d-wave superconductors. *Phys. Rev. B* 1995;51:15547. DOI: <http://dx.doi.org/10.1103/PhysRevB.51.15547>

- [40] Pogorelov YG, Ground state symmetry and impurity effects in superconductors. *Sol. St. Commun.* 1995;95:245-249. DOI: 10.1016/0038-1098(95)00260-X
- [41] Onari S, Kontani H. Violation of Anderson's Theorem for the Sign-Reversing s-Wave State in Iron-Pnictide Superconductors. *Phys. Rev. Lett.* 2009;103:177001. DOI: <http://dx.doi.org/10.1103/PhysRevLett.103.177001>
- [42] Kontani H, Onari S. Orbital-Fluctuation-Mediated Superconductivity in Iron Pnictides: Analysis of the Five-Orbital Hubbard-Holstein Model. *Phys. Rev. Lett.* 2010;104:157001. DOI: <http://dx.doi.org/10.1103/PhysRevLett.104.157001>
- [43] Efremov DV, Korshunov MM, Dolgov OV, Golubov AA, Hirschfeld PJ. Disorder-induced transition between s_{\pm} and s_{++} states in two-band superconductors. *Phys. Rev. B* 2011;84:180512. DOI: <http://dx.doi.org/10.1103/PhysRevB.84.180512>
- [44] Senga Y, Kontani H. Impurity Effects in Sign Reversing Fully-Gapped Superconductors: Analysis of FeAs Superconductors. *Journ. Phys. Soc. Japan* 2008;77:113710. DOI: 10.1143/JPSJ.77.113710
- [45] Kariado T, Ogata M. Single-Impurity Problem in Iron-Pnictide Superconductors. *Journ. Phys. Soc. Japan* 2010;79:083704. DOI: <http://dx.doi.org/10.1143/JPSJ.79.083704>
- [46] Beaird R, Vekhter I, Zhu JX, Impurity states in multiband s-wave superconductors: Analysis of iron pnictides. *Phys. Rev. B* 2012;86:140507. DOI: <http://dx.doi.org/10.1103/PhysRevB.86.140507>
- [47] Gordon RT, Kim H, Tanatar MA, Prozorov R, Kogan VG. London penetration depth and strong pair breaking in iron-based superconductors. *Phys. Rev. B* 2010;81:180501. DOI: <http://dx.doi.org/10.1103/PhysRevB.81.180501>
- [48] Kitagawa S, Nakai Y, Iye T, Ishida K, Guo YF, Shi YG, Yamaura K, Takayama-Muromachi E. Nonmagnetic pair-breaking effect in $\text{La}(\text{Fe}_{1-x}\text{Zn}_x)\text{AsO}_{0.85}$ studied by ^{75}As and ^{139}La NMR and NQR. *Phys. Rev. B* 2011;83:180501(R). DOI: <http://dx.doi.org/10.1103/PhysRevB.83.180501>
- [49] Guo YF, Shi YG, Yu S, Belik AA, Matsushita Y, Tanaka M, Katsuya Y, Kobayashi K, Nowik I, Felner I, Awana VPS, Yamaura K, Takayama-Muromachi E. Large decrease in the critical temperature of superconducting $\text{LaFeAsO}_{0.85}$ compounds doped with 3% atomic weight of nonmagnetic Zn impurities. *Phys. Rev. B* 2010;82:054506. DOI: <http://dx.doi.org/10.1103/PhysRevB.82.054506>
- [50] Li Y, Tong J, Tao Q, Feng C, Cao G, Chen W, Zhang F, Xu Z. Effect of a Zn impurity on T_c and its implications for pairing symmetry in $\text{LaFeAsO}_{1-x}\text{F}_x$. *New J. Phys.* 2010 ; 12 :083008. DOI : 10.1088/1367-2630/12/8/083008
- [51] Hardy F, Burger P, Wolf T, Fisher RA, Schweiss P, Adelman P, Heid R, Fromknecht R, Eder R, Ernst D, Löhnheysen Hv, Meingast C. Doping evolution of superconducting gaps and electronic densities of states in $\text{Ba}(\text{Fe}_{1-x}\text{Co}_x)_2\text{As}_2$ iron pnictides. *Europhys. Lett.* 2010;91:47008. DOI: 10.1209/0295-5075/91/47008

- [52] Loktev VM, Pogorelov YG. Formation of d-wave superconducting order in a randomly doped lattice. *Low Temp. Phys.* 2001;27:767-776. DOI: <http://dx.doi.org/10.1063/1.1401186>
- [53] Pogorelov YG, Santos MC, Loktev VM. Specifics of impurity effects in ferropnictide superconductors. *Phys. Rev. B* 2011;84:144510. DOI: <http://dx.doi.org/10.1103/PhysRevB.84.144510>
- [54] Pogorelov YG, Santos MC, Loktev VM. Green function study of impurity effects in high-Tc superconductors. In: Carmelo JMP, Lopes dos Santos JMB, Rocha Vieira V, Sacramento PD, editors. *Strongly Correlated Systems, Coherence and Entanglement*, World Scientific;2007. p. 443-494. ISBN 978-981-270-572-3. cap. 17
- [55] Kubo R. Statistical-Mechanical Theory of Irreversible Processes. I. General Theory and Simple Applications to Magnetic and Conduction Problems. *J. Phys. Soc. Jpn.* 1957 ;12 :570-586. DOI: <http://dx.doi.org/10.1143/JPSJ.12.570>
- [56] Greenwood DA. The Boltzmann Equation in the Theory of Electrical Conduction in Metals. *Proc. Phys. Soc.* 1958;71:585-596. DOI: 10.1088/0370-1328/71/4/306
- [57] Economou EN. *Green's Functions in Quantum Physics*. Springer, Berlin;2006. 477 p. DOI: 10.1007/3-540-28841-4
- [58] Mazin II, Schmalian J. Pairing symmetry and pairing state in ferropnictides: Theoretical overview. *Physica C* 2009;469:614-627. DOI:10.1016/j.physc.2009.03.019
- [59] DeWeert MJ. Proximity-effect bilayers with magnetic impurities: The Abrikosov-Gor'kov limit. *Phys. Rev. B* 1988;38:732-734. DOI: <http://dx.doi.org/10.1103/PhysRevB.38.732>
- [60] Srivastava RVA, Teizer W. Analytical density of states in the Abrikosov-Gorkov theory. *Solid State Commun.* 2008;145:512-513. DOI: 10.1016/j.ssc.2007.11.030
- [61] Note that this static limit of Eq. (47) only defines the conductivity by normal quasi-particles, seen e.g. in normal resistivity by the magnetic flux flow in the mixed state, but otherwise short circuited by the infinite static conductivity due to supercurrents.
- [62] Dolgov OV, Efremov DV, Korshunov MM, Charnukha A, Boris AV, Golubov AA. Multiband Description of Optical Conductivity in Ferropnictide Superconductors. *J. Supercond. Nov. Magn.* 2013;26:2637-2640. DOI: 10.1007/s10948-013-2150-3
- [63] Abramowitz MVL, Stegun IA, editors. *Handbook of Mathematical Functions With Formulas, Graphs, and Mathematical Tables*. Natl. Bureau of Standards;1964. 1046 p. ISBN 0-486-61272-4 DOI: 10.2307/2008636
- [64] Broude, Prikhot'ko AF, Rashba EI. Some problems of crystal luminescence. *Sov. Phys. Uspekhi* 1959;2:38-49. DOI: <http://dx.doi.org/10.1070/PU1959v002n01ABEH003107>